Master-Slave Locking of Optomechanical Oscillators over a Long Distance

Shreyas Y. Shah,[1] Mian Zhang,[1] Richard Rand,[2,3] and Michal Lipson[1,4]

[1]*School of Electrical and Computer Engineering, Cornell University, Ithaca, New York 14853, USA*
[2]*Department of Mathematics, Cornell University, Ithaca, New York 14853, USA*
[3]*Sibley School of Mechanical and Aerospace Engineering, Cornell University, Ithaca, New York 14853, USA*
[4]*Kavli Institute at Cornell for Nanoscale Science, Ithaca, New York 14853, USA*

Frequency locking and other phenomena emerging from nonlinear interactions between mechanical oscillators are of scientific and technological importance. However, existing schemes to observe such behavior are not scalable over distance. We demonstrate a scheme to couple two independent mechanical oscillators, separated in frequency by 80 kHz and situated far from each other (3.2 km), via light. Using light as the coupling medium enables this scheme to have low loss and be extended over long distances. This scheme is reversible and can be generalized for arbitrary network configurations.

Frequency locking between micromechanical oscillators is critical for RF communication and signal-processing applications [1–3]; however, its scalability is limited by the fact that, in general, the oscillators are obliged to be in physical proximity in order to interact. Micromechanical oscillators can interact at the micron scale via electronic coupling [4] or a physical connection [5]. However, these schemes are fundamentally lossy over long distances, and therefore, are not scalable. Scaling up coupled mechanical oscillators to macroscale networks [6–8] could potentially enable novel concepts in memory and computation [9–11], as well as provide a platform to put in practice many theories of nonlinear dynamics of coupled oscillators [12,13].

Interaction of mechanical oscillators through light could, in principle, help overcome this limitation, since light can propagate over long distances with minimal loss. Recent reports [5,14,15] on frequency locking between mechanical oscillators demonstrate interaction only over a few micrometers. In demonstrations of light-mediated coupling of two micromechanical oscillators [14,15], both mechanical oscillators are coupled to the same optical cavity, limiting the kind of network topologies that can be used and how far the oscillators can be separated.

In this Letter, we demonstrate a reconfigurable scheme to couple, via light, two independent micromechanical oscillators separated from each other by an effective path of 3.2 km, in the master-slave configuration and show the ability to lock their oscillation frequencies. This coupling scheme is based on using light to send the information of the mechanical oscillations from the master oscillator to the slave oscillator. It is facilitated by the fact that each oscillator is an optomechanical oscillator (OMO), consisting of colocalized optical resonances and mechanical resonances that are coupled to each other [see Eqs. (1a) and (1b)] [16]. The mechanical resonator can be modeled as a damped simple harmonic oscillator with position x,

effective mass m_{eff}, frequency Ω_m, and damping rate Γ_m. It is driven by its interaction with an optical force $F_{\mathrm{opt}} = g_{\mathrm{om}}(|a|^2/\omega)$, where $|a|^2$ is the energy in the optical cavity and ω is the laser frequency. g_{om} indicates the strength of the interaction between optics and mechanics. The optical cavity can also be modeled as a damped oscillator, with a position-dependent frequency $(\omega_0 + g_{\mathrm{om}}x)$ and damping rate Γ_{opt}, and it is driven with a laser of power $|s|^2$, coupled to the cavity at the rate Γ_{ex}. The force on the mechanical resonator F_{opt} can be controlled by changing the intracavity energy $|a|^2$, which is, in turn, affected by the laser power $|s|^2$. Any modulation of the laser power therefore couples to the mechanical resonator via the optical force F_{opt} [17],

$$\frac{da}{dt} = i[(\omega - \omega_0) - g_{\mathrm{om}}x]a - \Gamma_{\mathrm{opt}}a + \sqrt{2\Gamma_{\mathrm{ex}}}s, \quad (1\mathrm{a})$$

$$\frac{d^2x}{dt^2} + \Gamma_m\frac{dx}{dt} + \Omega_m^2 x = \frac{F_{\mathrm{opt}}[a]}{m_{\mathrm{eff}}}. \quad (1\mathrm{b})$$

The OMOs used for this demonstration each consist of two suspended Si_3N_4 microdisks stacked vertically [Figs. 1(a) and 1(b)]. The optical and mechanical resonances under consideration are colocalized along the periphery of the structure. These structures are fabricated using e-beam lithography techniques [14]. The top and bottom Si_3N_4 disks are nominally 250 nm and 220 nm thick and have a radius of 20 μm. These disks are separated from each other by a 170-nm-thick SiO_2 sacrificial spacer layer. This stack rests on a 4-μm-thick SiO_2 support layer. These layers are partially etched away to release the periphery of these disks. This suspended structure supports optical whispering-gallery modes that overlap with the edges of the top and bottom disks [Fig. 1(a)] [14]. The optical resonance frequency of this structure is strongly dependent on the separation between the two disks.
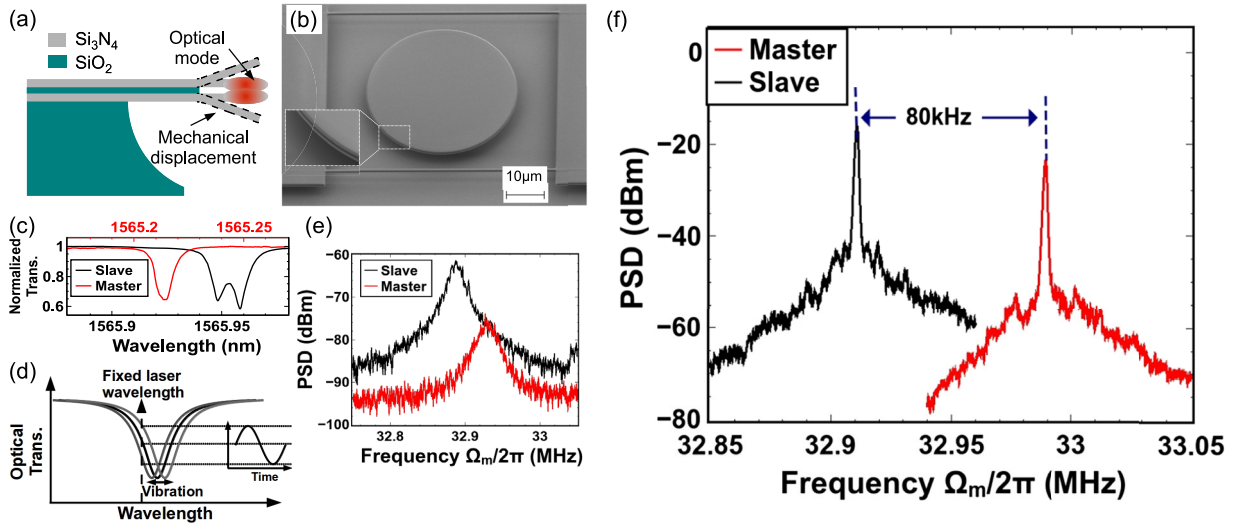
FIG. 1 (color online).   (a) Schematic depiction of cross section of the device, indicating the colocalization of optical and mechanical resonances. The dotted line indicates the relative mechanical displacement between the two disks that influences the optical mode. (b) SEM image of the optomechanical (OM) resonator. Inset: higher-magnification SEM image of the region highlighted, showing the double-microdisk structure. (c) Normalized transmission spectra of master and slave optical resonances. (d) Vibration of the mechanical resonator causes the optical resonance to vibrate about a mean value, resulting in modulation of transmitted optical power. (e) Power spectral density (PSD) of the modulation of the transmitted optical power due to thermally induced mechanical vibration shows the natural frequency of the mechanical resonator. (f) PSD of master and slave oscillations. The oscillation peaks are offset by 80 kHz.

Relative motion [represented by Eq. (1b)] between the two disks changes the resonance frequency at the rate of $g_{om} = -2\pi \times 49$ GHz/nm, as calculated from finite element simulations [14].

The two devices, when not coupled, oscillate at two distinct mechanical frequencies separated by 80 kHz. In order to characterize the devices, light is coupled into each resonator with a tapered optical fiber. The transmission spectrum of the master OM resonator shows an optical resonance centered at ∼1565.22 nm [Fig. 1(c)]. Similarly, the slave OM resonator has an optical resonance centered at ∼1565.95 nm [Fig. 1(c)]. The splitting in the resonance is due to backscattering-induced lifting of degeneracy between the clockwise and counterclockwise propagating modes [18]. Thermal motion of the mechanical resonators modulates this transmission spectrum [Fig. 1(d)], which can be analyzed with a spectrum analyzer. The master is observed to have a mechanical resonance at 33.93 MHz [Fig. 1(e)], with a linewidth of 16.39 kHz, while the slave has a mechanical resonance centered at 32.82 MHz [Fig. 1(e)], with a linewidth of 13.56 kHz. When the optical resonances are excited with blue-detuned lasers ($\omega > \omega_0$), dynamical backaction [16] amplifies mechanical motion. As input power is increased, this mechanical gain increases, until it overcomes intrinsic mechanical damping. At this point, each resonator becomes a self-sustaining oscillator [16]. The master oscillates at 32.99 MHz [Fig. 1(f)], and the slave oscillates independently at 32.91 MHz [Fig. 1(f)], i.e., separated from the master by more than 6 times its natural mechanical linewidth. Note that, due to the optical-spring

effect [16], the oscillation frequencies for the oscillators are centered at a frequency slightly higher than that for the thermal motion of the respective resonator.

To demonstrate long-distance locking, we couple the two OMOs in a master-slave configuration, via a 3.2-km-long optical fiber, with an electro-optic modulator that is driven by the master OMO and that modulates the laser driving the slave OMO [see Fig. 2 and Eq. (2)]. Each OMO is pumped by an independent laser. The signal transmitted from the master OMO carries information about its position x_{master}. It travels through a 3.2-km-long delay line before it is detected with a high-speed detector. The output of this detector carries the RF oscillations, which are a function of the mechanical displacement x_{master} of the master. The slave laser drive s_{slave} is modulated by this signal from the master [Eq. (2)]. The output of the slave OMO is detected with another high-speed detector and analyzed with a spectrum analyzer and an oscilloscope,

$$|s_{slave}|^2 = |s_{0,slave}|^2 (1 + \gamma[f(x_{master})]). \tag{2}$$

The strength of coupling between the slave OMO and the output of the master OMO can be controlled by the modulation depth γ of the electro-optic modulator driven by the master oscillator. A voltage-controlled variable-gain amplifier provides a gain between -26 dB and $+35$ dB to the RF oscillations coming from the detector of the master OMO, and thereby controls the modulation depth. This is reflected in the PSD of the oscillation peak of the master
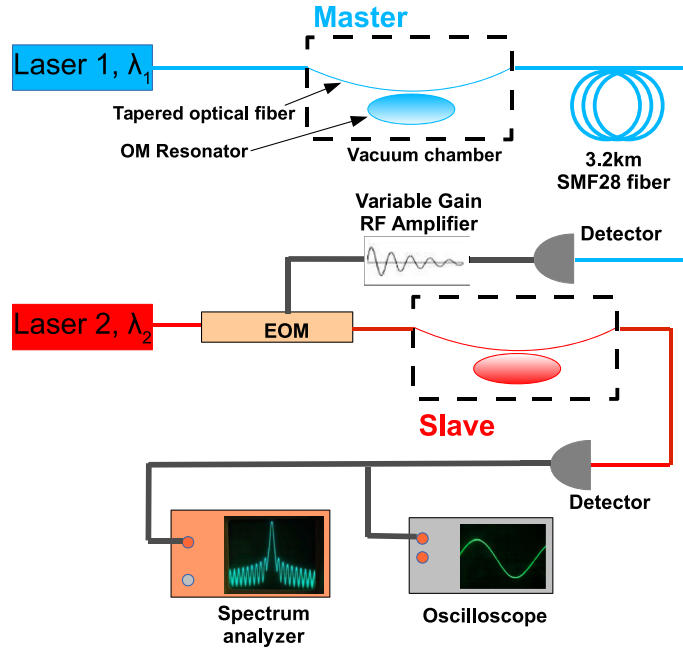
FIG. 2 (color online).   Schematic of experimental setup to demonstrate master-slave locking. The two optomechanical (OM) resonators are driven by independent lasers. The optical signal from the master travels through 3.2 km of single mode fiber (SMF). The RF signal generated at the detector by the oscillations of the master modulates, via an electro-optic modulator (EOM), the laser driving the slave. The RF oscillations of the slave are analyzed with a spectrum analyzer and an oscilloscope.

OMO (H_{inj}) as seen in the light transmitted from the slave OMO [Fig. 3(a)].

As we increase the coupling strength, we show that the slave OMO transitions from oscillating independently to being frequency locked to the master OMO. The coupling strength is determined by comparing the amount of modulation imparted on $|s_{slave}|^2$ by the injected signal and by the slave oscillator. This is measured in terms of the ratio of the power of injected oscillation signal (H_{inj}) to the power of the free-running slave oscillation (H_{slave}). When H_{inj}/H_{slave} is small, the slave OMO oscillates at its own frequency, independently. The optical signal transmitted from the slave carries the slave oscillation peak, along with the modulation imparted on the laser [Fig. 3(a)]. As the injection strength is increased, the slave oscillation frequency is pulled toward the master oscillation frequency. After a transition point ($H_{inj}/H_{slave} \sim -2$ dB), the slave OMO spontaneously begins oscillating at the same frequency as the master OMO.

We show that frequency locking can also occur when the roles of the slave and the master are reversed [Fig. 3(c)]. As we increase the coupling strength, the new slave spontaneously begins oscillating at the same frequency as the new master after a transition point around $H_{inj}/H_{slave} \sim 8$ dB. The difference in the locking strength for each of the oscillators can be attributed to the strongly nonlinear nature of these oscillators [19] (see the Supplemental Material [20]). We observe phase locking between the master and the slave oscillators when their frequencies lock. The locking transition is associated with the establishment of

a fixed phase relationship between the master and the slave oscillations. We can observe the change in the phase relationship upon locking between the master and slave oscillators by plotting the oscillation signal of the slave versus that of the master, over a duration long enough to accommodate phase drift. When the slave OMO is free-running, its phase is uncorrelated to the phase of the master OMO. As a result, for each point in the phase space of the master OMO, the phase of the slave OMO can take any value in its range (i.e., 0° to 360°). This is reflected in the phase portrait of the oscillations of the master OMO and slave OMO forming a filled rectangle [Fig. 4(a)], over an extended period of time (4 μs, i.e., more than 130 oscillation cycles) [32]. When the slave OMO is locked to the master OMO, the phase difference between the two oscillations is fixed, and the phase perturbations (phase noise) are correlated (see the Supplemental Material [20]). This correlation between the phases of the two oscillators results in the x-y trace of the oscillations [Fig. 4(b)] of the master and slave OMOs forming an open Lissajous figure [32].

Full numerical simulations of Eqs. (1) and (2) for the master and slave OMOs confirm the observation of locking [Figs. 3(b) and 3(d)]. The dynamics of the slave OMO and the master OMO are simulated with experimentally derived parameters. The set of coupled optical and mechanical equations [Eqs. (1a) and (1b)] are numerically integrated using commercially available software [14,20]. The power in the optical drive for the slave $|s_{slave}|^2$ [Eq. (2)] in the simulation contains a signal $\gamma[f(x_{master})]$, which is
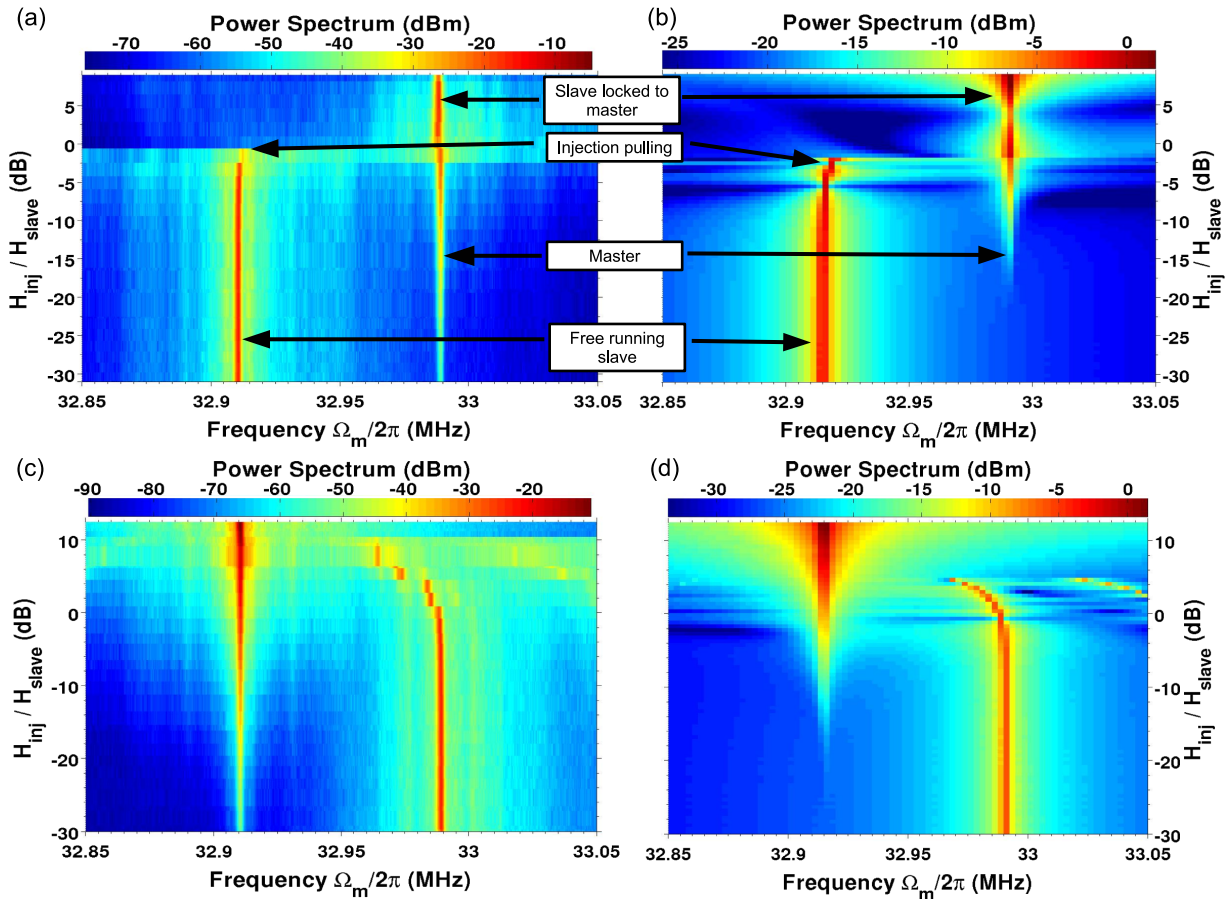
FIG. 3 (color online).   (a) Spectrum of the power transmitted from the slave OMO for different injection ratios (H_{inj}/H_{slave}).
(b) Numerical simulation of the power spectrum. (c),(d) Same as (a) and (b), respectively, only now measured by reversing the roles
of master and slave.

proportional to the transmitted signal from the master
OMO. As the gain is increased, the slave is locked to
the oscillations of the master OMO. The simulations also
reproduce, qualitatively, major features of the dynamics,
including injection pulling [33].

Our demonstration of master-slave locking of two
OMOs separated by kilometers of fiber utilizes a

reconfigurable coupling scheme that can be easily
extended to include mutual coupling between the two
oscillators as well as to implementing a large network of
oscillators with arbitrary network topologies. The ability
to tune the coupling strength arbitrarily enables access to
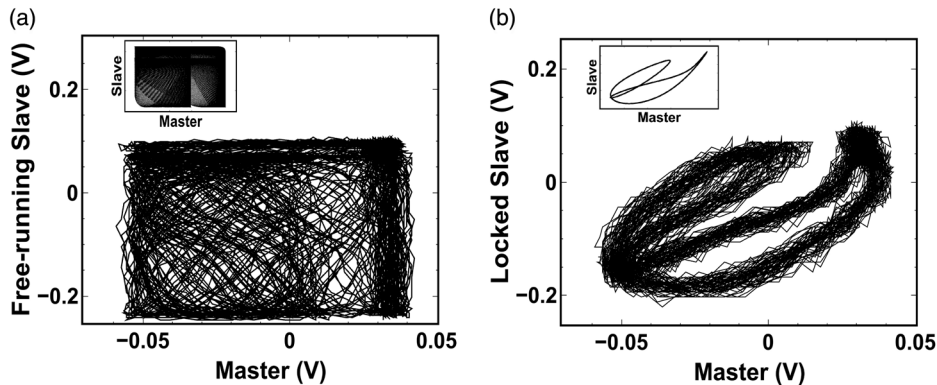various regimes of nonlinear dynamics of such oscillator
networks.

FIG. 4.   Phase portraits formed by the oscillation signals of the (a) free-running slave and (b) locked slave with the master oscillator,
as measured with an oscilloscope, over more than 130 oscillation cycles. Insets: simulated phase portraits.

P H Y S I C A L   R E V I E W   L E T T E R S

---

[1] S. Strogatz, *Sync: The Emerging Science of Spontaneous Order* (Hyperion, New York, 2003).

[2] S. Bregni, *Synchronization of Digital Telecommunications Networks* (Wiley, New York, 2002).

[3] K. Stephan, IEEE Trans. Microwave Theory Tech. **34**, 1017 (1986).

[4] M. H. Matheny, M. Grau, L. G. Villanueva, R. B. Karabalin, M. C. Cross, and M. L. Roukes, Phys. Rev. Lett. **112**, 014101 (2014).

[5] S.-B. Shim, M. Imboden, and P. Mohanty, Science **316**, 95 (2007).

[6] A. Tomadin, S. Diehl, M. D. Lukin, P. Rabl, and P. Zoller, Phys. Rev. A **86**, 033821 (2012).

[7] M. Ludwig and F. Marquardt, Phys. Rev. Lett. **111**, 073603 (2013).

[8] G. Heinrich, M. Ludwig, J. Qian, B. Kubala, and F. Marquardt, Phys. Rev. Lett. **107**, 043603 (2011).

[9] I. Mahboob and H. Yamaguchi, Nat. Nanotechnol. **3**, 275 (2008).

[10] M. Bagheri, M. Poot, M. Li, W. P. H. Pernice, and H. X. Tang, Nat. Nanotechnol. **6**, 726 (2011).

[11] F. Hoppensteadt and E. Izhikevich, IEEE Trans. Circuits Systems **48**, 133 (2001).

[12] C. Joshi, J. Larson, M. Jonson, E. Andersson, and P. Ohberg, Phys. Rev. A **85**, 033805 (2012).

[13] D. V. Ramana Reddy, A. Sen, and G. L. Johnston, Phys. Rev. Lett. **80**, 5109 (1998).

[14] M. Zhang, G. S. Wiederhecker, S. Manipatruni, A. Barnard, P. McEuen, and M. Lipson, Phys. Rev. Lett. **109**, 233906 (2012).

[15] M. Bagheri, M. Poot, L. Fan, F. Marquardt, and H. X. Tang, Phys. Rev. Lett. **111**, 213902 (2013).

[16] T. J. Kippenberg and K. J. Vahala, Opt. Express **15**, 17172 (2007).

[17] M. Hossein-Zadeh and K. J. Vahala, Appl. Phys. Lett. **93**, 191115 (2008).

[18] T. J. Kippenberg, S. M. Spillane, and K. J. Vahala, Opt. Lett. **27**, 1669 (2002).

[19] M. Zalalutdinov, K. L. Aubin, M. Pandey, A. T. Zehnder, R. H. Rand, H. G. Craighead, J. M. Parpia, and B. H. Houston, Appl. Phys. Lett. **83**, 3281 (2003).

[20] See Supplemental Material at http://link.aps.org/supplemental/10.1103/PhysRevLett.114.113602, which includes Refs. [21–31], for a theoretical analysis of the locking process, and additional data on locking dynamics.

[21] H. A. Haus, *Waves and Fields in Optoelectronics* (Prentice Hall, Englewood Cliffs, NJ, 1984).

[22] R. W. Boyd, *Nonlinear Optics* (Academic Press, New York, 2008).

[23] M. Abramowitz and I. A. Stegun, *Handbook of Mathematical Functions: With Formulas, Graphs, and Mathematical Tables* (Courier Dover, New York, 2012).

[24] R. Adler, Proc. IRE **34**, 351 (1946).

[25] R. H. Rand, Lecture Notes on Nonlinear Vibrations, http://hdl.handle.net/1813/28989.

[26] M. Pandey, R. H. Rand, and A. T. Zehnder, Nonlinear Dyn. **54**, 3 (2008).

[27] F. Marquardt, J. G. E. Harris, and S. M. Girvin, Phys. Rev. Lett. **96**, 103901 (2006).

[28] K. Kurokawa, IEEE Trans. Microwave Theory Tech. **16**, 234 (1968).

[29] H.-C. Chang, X. Cao, M. Vaughan, U. K. Mishra, and R. York, IEEE Trans. Microwave Theory Tech. **45**, 2035 (1997).

[30] H.-C. Chang, X. Cao, U. K. Mishra, and R. York, IEEE Trans. Microwave Theory Tech. **45**, 604 (1997).

[31] H. Rokhsari, M. Hossein-Zadeh, A. Hajimiri, and K. Vahala, Appl. Phys. Lett. **89**, 261109 (2006).

[32] A. Pikovsky and J. Kurths, *Synchronization: A Universal Concept in Nonlinear Sciences* (Cambridge University Press, Cambridge, England, 2003).

[33] B. Razavi, IEEE J. Solid-State Circuits **39**, 1415 (2004).

Master-Slave Locking of Optomechanical Oscillators Over A Long Distance

Shreyas Y. Shah,[1] Mian Zhang,[1] Richard Rand,[2,3] and Michal Lipson[1,4]

[1]*School of Electrical and Computer Engineering,*

Cornell University, Ithaca, New York 14853, USA

[2]*Department of Mathematics, Cornell University, Ithaca, New York 14853, USA*

[3]*Sibley School of Mechanical and Aerospace Engineering,*

Cornell University, Ithaca, New York 14853, USA

[4]*Kavli Institute at Cornell for Nanoscale Science, Ithaca, New York 14853, USA*

THE OPTOMECHANICAL OSCILLATOR

An optomechanical oscillator can be described by a set of coupled equations describing the optical mode (S1(a)) and the mechanical mode (S1(b)). The main text provides a physical description of these equations.

$$\frac{da}{dt} = i(\Delta_0 - g_{om}x)a - \Gamma_{opt}a + \sqrt{2\Gamma_{ex}}s \tag{S1(a)}$$

$$\frac{d^2x}{dt^2} + \Gamma_m\frac{dx}{dt} + \Omega_m^2 x = \frac{F_{opt}[a]}{m_{eff}} \tag{S1(b)}$$

In the 'bad cavity limit', i.e. in the case where the optical decay rate Γ_{opt} is much larger than the mechanical frequency ($\Gamma_{opt} \gg \Omega_m$), for a given displacement x, the optical cavity reaches a steady state much faster than the mechanical resonator responds to the change in $F_{opt}[a]$ $\left(= \frac{g_{om}|a|^2}{\omega}\right)$. Therefore, in this limit, one may analyse Eq. S1(a) quasistatically, with a value of x delayed by the response-time $\tau(= \frac{1}{\Gamma_{opt}})$ of the optical cavity. This delay accounts for the fact that although the optical cavity responds much faster than the mechanical resonator, it does not do so instantaneously. Therefore, the steady state value for a is given by Eq. S2, and substituting it in Eq. S1(b) yields an equation for mechanical motion (Eq. S2(b)) in the quasistatic approximation for the optical cavity.

$$a(t) = \frac{\sqrt{2\Gamma_{ex}}s}{i(\Delta_0 - g_{om}x(t-\tau)) - \Gamma_{opt}} \tag{S2(a)}$$

$$\frac{d^2x(t)}{dt^2} + \Gamma_m\frac{dx(t)}{dt} + \Omega_m^2 x(t) = \frac{g_{om}}{m_{eff}\omega}\frac{2|s|^2\Gamma_{ex}}{(\Delta_0 - g_{om}x(t-\tau))^2 + \Gamma_{opt}^2} \tag{S2(b)}$$

Eq. S2(b) can be simplified by normalising the displacement ($y = \frac{g_{om}x}{\Delta_0}$) and time ($T = t\Omega_m$), and substituting $A = \frac{2g_{om}^2\Gamma_{ex}}{m_{eff}\omega\Omega_m^2\Delta_0^3}$, $B = (\frac{\Gamma_{opt}}{\Delta_0})^2$, and $Q_m = \frac{\Omega_m}{\Gamma_m}$, to give

$$\frac{d^2y(T)}{dT^2} + \frac{1}{Q_m}\frac{dy(T)}{dT} + y = \frac{A|s|^2}{B + (1 + y(T - \tau\Omega_m))^2} \tag{S3}$$

OSCILLATION POWER AND INJECTION RATIO

When an optomechanical cavity is excited with a laser of power $|s|^2$ via a waveguide coupled to the optical cavity with a coupling constant $\sqrt{2\Gamma_{ex}}$, the power exiting the cavity is given by $|s_{out}|^2 = |s - \sqrt{2\Gamma_{ex}}a|^2$ [1]. Using Eq. S2(a), and letting D_g represent the

2

transimpedance gain of the detector and input gain of the spectrum analyzer, the power detected at the spectrum analyzer can be written as

$$P_{trans}(x) = D_g |s|^2 |1 - \frac{2\Gamma_{ex}}{i(\Delta_0 - g_{om}x) - \Gamma_{opt}}|^2 \tag{S4}$$

If x oscillates at the frequency Ω_{osc} i.e. $x = x_0 \cos(\Omega_{osc}t)$, P_{trans} can be approximated in terms of its spectral components, i.e. as a Fourier series Eq. S5, where $D_g|s|^2(P_0, P_1, P_2, ...)$ are the power-spectral-density (PSD) values of P_{trans} at the frequencies $(0, \Omega_{osc}, 2\Omega_{osc}, ...)$. This approximation holds because the linewidth reduces dramatically when oscillations begin [2], and most of the power in the spectral component is concentrated at the centre-frequency itself. Harmonics are introduced because of the non-linear transduction between x and P_{trans}. It must be noted that $(P_0, P_1, P_2, ...)$ are functions of x_0 since they are Fourier coefficients of $|1 - \frac{2\Gamma_{ex}}{i(\Delta_0 - g_{om}x) - \Gamma_{opt}}|^2$

$$P_{trans} = D_g|s|^2 (P_0 + P_1 \cos(\Omega_{osc}t) + P_2 \cos(2\Omega_{osc}t) + ...) \tag{S5}$$

The parameter H_{slave} from the main text can, therefore, be written as $H_{slave} = D_{g,slave}|s_{slave}|^2 P_{1,slave}$. This value is directly read off the spectrum analyzer.

The output of the master oscillator modulates the laser driving the slave, as per Eq. 2 in the main text (Also see section 'Electro-optic coupling'). The modulation function $f(x_{master})$ is proportional to Eq. S5, where all the PSD values correspond to the master oscillator. Assuming that the harmonics are negligible compared to the fundamental frequency component i.e. coefficient of $\cos(\Omega_{inj}t)$, Eq. 2 from the main text can be rewritten as Eq. S6, where the detector transimpedance gain $D_{g,master}$, propagation loss, modulation gain from the electro-optic modulator and the variable RF amplifier gain, are absorbed into the variable parameter γ.

$$|s_{slave}|^2 = |s_{0,slave}|^2(1 + \gamma \cos(\Omega_{inj}t)) \tag{S6}$$

$$P_{trans,slave} = D_{g,slave}|s_{0,slave}|^2(1 + \gamma \cos(\Omega_{inj}t))(P_{0,slave} + P_{1,slave} \cos(\Omega_{osc}t) + P_{2,slave} \cos(2\Omega_{osc}t) + ...) \tag{S7}$$

Substituting Eq. S6 in Eq. S5 gives Eq. S7, from which we can find the PSD of $P_{trans,slave}$ at the frequency Ω_{inj}. The parameter H_{inj} from the main text can, therefore, be written as $H_{inj} = D_{g,slave}|s_{slave}|^2 P_{0,slave}\gamma$. This value, too, is directly read off the spectrum analyzer.

3

Therefore, the injection ratio $\frac{H_{inj}}{H_{slave}}$ equals the ratio of the relative amplitudes of modulations of the optical power in the waveguide (i.e. ratio of modulation depths), caused by injected signal and the free-running slave oscillator, i.e.

$$\frac{H_{inj}}{H_{slave}} = \frac{\gamma}{P_1/P_0} \tag{S8}$$

Electro-optic coupling

We use an electro-optic modulator to couple master oscillator to the slave oscillator. The RF power transmitted from the master oscillator ($P_{trans,master}$) modulates the optical power transmitted through the modulator as per Eq. S9(a) [3], where Γ accounts for the gain of the amplifier (see main text) and the modulator.

$$|s|^2 = |s_0|^2(1 + \frac{1}{2}\sin(\Gamma P_{trans,master})) \tag{S9(a)}$$

$$|s|^2 = |s_0|^2(1 + \frac{\Gamma}{2}P_{trans,master}) \tag{S9(b)}$$

For sufficiently small values of $\Gamma P_{trans,master}$, Eq. S9(a) can be written as Eq. S9(b). For a sinusoidal variation of $P_{trans,master}$ (Eq. S6), the modulation term on the RHS of Eq. S9(a) can be expanded in terms odd harmonics of Ω_{inj} [4]. Therefore, the smallest harmonic corresponds to $3\Omega_{inj}$, and the component corresponding to $2\Omega_{inj}$ is absent.

FREQUENCY-LOCKING OF OPTOMECHANICAL OSCILLATORS

Optomechanical back-action [2], which amplifies or dampens mechanical oscillations, occurs because the optical-force has a component in phase with the velocity of the mechanical resonator. This is because the optical cavity does not respond instantaneously (i.e. $\tau \neq 0$). However, this also makes analysing Eq. S3 and frequency-locking difficult, because it is a delay-differential equation.

The oscillation amplitude and phase (frequency) of optomechanical oscillators are not mutually independent, as demonstrated by the optomechanical spring effect [2]. As a result, the well-known Adler equation [5, 6] which models injection-locking of oscillators via

phase-only coupling, does not adequately reflect the dynamics of locking of optomechanical oscillators represented by Eq. S3.

In this section, we will reduce Eq. S3, under appropriate approximations, to a variant of the well-known Mathieu equation [7], which will serve as a template to understand locking behaviour in optomechanical oscillators.

Simplfied Model Based on Mathieu Equation

The optomechanical oscillator begins undergoing self-sustained oscillations (limit-cycle oscillations) as the laser power crosses a threshold value which is determined by $\frac{1}{Q_m}, A, B$ and τ [2]. Below this threshold laser power, oscillation-amplitude decays due to mechanical damping. If we neglect damping, i.e. $\frac{1}{Q_m} = 0$, we can assume $\tau = 0$ and still have oscillatory solutions to the equation, with a sustained oscillation-amplitude. This gives us

$$\frac{d^2y}{dT^2} + y = \frac{A|s|^2}{B + (1+y)^2} \tag{S10}$$

When damping is neglected, even small values of y (i.e. the change in optical resonance frequency caused by mechanical motion is much smaller than the linewidth of the optical resonance) correspond to oscillatory motion. Therefore, Eq. S10 can be further simplified by assuming $y \ll 1$, and considering only the first three terms from the Taylor expansion of the RHS around $y = 0$, giving Eq. S11. We include the lowest-order nonlinear term (i.e. the quadratic term) to analyse the effect of nonlinearity in locking, and include amplitude-frequency coupling in the analysis.

$$\frac{d^2y}{dT^2} + y = \frac{A|s|^2}{(1+B)^3}((1+B)^2 - 2(1+B)y - (B-3)y^2) \tag{S11}$$

The laser power $|s|^2$ is modulated by an external signal from the master oscillator, as per Eq. S6. Substituting this in Eq. S11, and rearranging terms gives Eq. S12, where $E_1 = 2\frac{A|s_0|^2}{(1+B)^2}, E_2 = \frac{(B-3)E_1}{2(1+B)}, E_0 = (1+B)\frac{E_1}{2}, \Omega = \frac{\Omega_{inj}}{\Omega_m}$.

$$\frac{d^2y}{dT^2} + (1 + E_1 + \gamma E_1 \cos(\Omega T))y + \gamma \cos(\Omega T)E_2 y^2 = E_0(1 + \gamma \cos(\Omega T)) \tag{S12}$$

Eq. S12 represents a forced oscillator, with parametric as well as non-parametric forcing. Note that we neglect the unforced quadratic term $E_2 y^2$ on the LHS while deriving Eq. S12

5

because, in practice, $E_2 \ll 1$, and the unforced motion is essentially simple harmonic. Non-parametric forcing of a linear oscillator gives a response at the forcing frequency, along with the natural frequency. The solution is altered only when the detuning i.e. difference between natural frequency and forcing frequency is zero. However, this case is not of interest, since we are looking for the response of the oscillator when the detuning is not zero.

Parametric forcing can lead to instability due to the parametric-resonance phenomenon [7]. These unstable oscillations are at the same frequency as the forcing frequency [7] i.e. the instability corresponds to locked oscillations. As the oscillation amplitude increases, higher-order terms, which were neglected in Eq. S11 become significant, and limit the oscillation amplitude. However, in order to study locking, it is sufficient to study Eq. S12 without the non-parametric forcing. Eq. S13 is similar to Mathieu's equation [7], and can be analysed using perturbation theory, with γ as the perturbation parameter, $U = \Omega T, \delta = \delta_0 + \gamma \delta_1 + \gamma^2 \delta_2, \delta_0 = \frac{1+E_1}{\Omega^2}, D_1 = \frac{E_1}{\Omega^2}, D_2 = \frac{E_2}{\Omega^2}, y = y_0 + \gamma y_1 + \gamma^2 y_2$

$$\frac{d^2y}{dU^2} + (\delta + \gamma D_1 \cos(U))y + \gamma \cos(\Omega T)D_2 y^2 = 0 \tag{S13}$$

We use the method of multiple time scales [7] to analyse Eq. S13, with $\xi = U, \eta = \gamma U, \nu = \gamma^2 U$, around the parametric resonance occuring at $\delta_0 = 1$ (i.e. when forcing frequency is close to the frequency of the oscillator). Note that this case is different from the stardard analysis of parametric excitation when the excitation frequency is close to twice the oscillator frequency. Also see the section 'Electro-optic coupling'.

For a given value of normalised detuning $\Delta(= 1 - \sqrt{\delta})$ between the oscillator frequency and the forcing frequency, the perturbation parameter γ is obtained from Eq. S14.

$$\gamma^2 \delta_2 + \gamma \delta_1 + 1 - (1 - \Delta)^2 = 0 \tag{S14}$$

Upon performing the perturbation analysis and finding conditions for the solution to be stable in each order of perturbation, we get expressions for δ_1 and δ_2 (Eqs. S15), which represent the curves along the boundary of regions of locked and unlocked oscillations i.e. the Arnold tongue (R is the unperturbed oscillation amplitude of Eq. S13).

$$\delta_1 = -\frac{3}{4}D_2 R, \delta_2 = \frac{5}{6}D_1(\frac{D_1}{2} + D_2 R) \tag{S15(a)}$$

$$\delta_1 = \frac{3}{4}D_2 R, \delta_2 = \frac{5}{6}D_1(\frac{D_1}{2} - D_2 R) \tag{S15(b)}$$

6

Substituting Eqs. S15 in Eq. S14 and solving Eq. S14 for γ, we get the minimum value of γ necessary to lock the slave oscillator with a detuning of Δ.

Arnold tongue for frequency locking

The injection ratio $\dfrac{H_{inj}}{H_{slave}}$ is given by Eq. S8, where P_0 and P_1 are the Fourier components of $|1 - \dfrac{2\Gamma_{ex}}{i(\Delta_0 - g_{om}x) - \Gamma_{opt}}|^2$ at the frequencies 0 and Ω_{inj}. Taking $x = x_0 \cos(\Omega_{osc}t)$, we find from the Taylor expansion of $|1 - \dfrac{2\Gamma_{ex}}{i(\Delta_0 - g_{om}x) - \Gamma_{opt}}|^2$ around $x = 0$,

$$\frac{P_1}{P_0} \approx \frac{8\Delta_0 g_{om}\Gamma_{ex}(\Gamma_{opt} + \Gamma_{ex})x_0}{(\Gamma_{opt}^2 + \Delta_0^2)((\Gamma_{opt} + 2\Gamma_{ex})^2 + \Delta_0^2)} \tag{S16}$$

Substituting experimental and simulated [8] values in Eqs. S14, S15 and S16, and $x_0 = 10^{-11}$m [9], we get Fig. S1, representing the Arnold tongue (as a function of modulation depth γ and normalised detuning Δ) for the locking of slave oscillator to the master oscillator. The red and blue lines on the figure indicate the detuning of the oscillators used in the experiment.

Comparison with experiment

It is remarkable that despite the extreme simplicity of the model used, it shows the expected trend for the minimum injection ratio required to lock as detuning increases. The values of injection ratios for locking obtained from the model, for the frequency detuning of oscillators in the experiment, are withing 5dB of experimental values. The role played by the nonlinear term is obvious from the inset of Fig. S1, which shows the Arnold tongue obtained by performing perturbation analysis on Eq. S13 with $D_2 = 0$. Without the nonlinear term coupling the amplitude and frequency, the minimum injection ratios obtained from the analysis are 10dB and 14dB larger than experimental values.

It must be emphasised that Eq. S13 is suitable only to understand the essential features of the locking process i.e. the Arnold tongue and the role played by nonlinearities. A better match between analytical and experimental results may be obtained by considering more terms in the expansion in Eq. S11. Specifically, the difference in the locking strength required
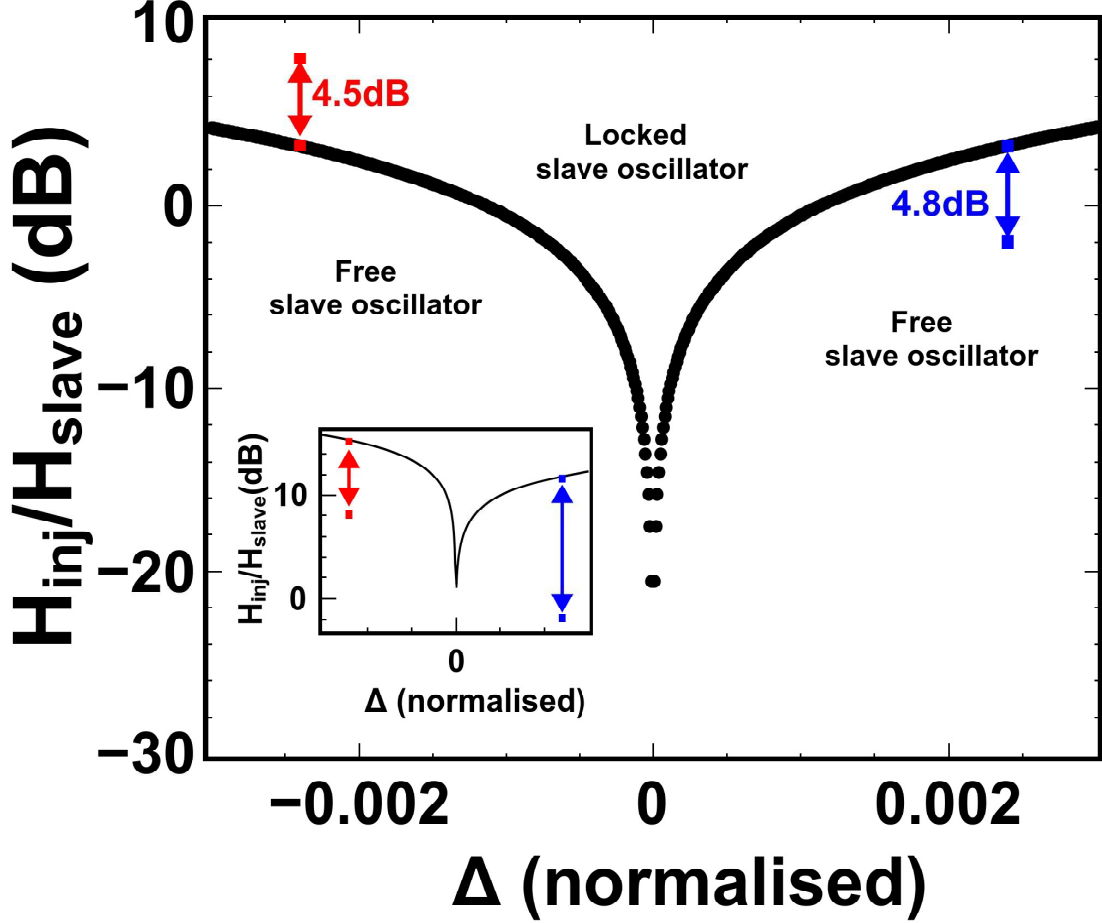
Figure S1. Plot of the Arnold tongue i.e. the minimum value of $\dfrac{H_{inj}}{H_{slave}}$ required for locking, as a function of normalised detuning $\Delta \; (= 1 - \dfrac{\Omega_{slave}}{\Omega_{inj}})$, obtained from Eqs. S8, S14, S15 and S16. The red and blue points **on the curve** indicate locking thresholds obtained from the analysis for the detuning of the oscillators in the main text. The arrows show that that the errors between experimental and analytical values for locking thresholds are less than 5dB. The analysis does not hold at $\Delta = 0$, and that point is not included in the plot. Inset shows the tongue obtained by neglecting all quadratic terms.

upon switching the roles of the master and slave oscillators, as seen in the experiment, may be obtained in this model by considering higher nonlinear terms, which are known to induce an asymmetrical response [10, 11]. One may go a step further and even attempt to analyse Eq. S3 as a delay-differntial equation. However, the analysis is significantly more challenging and beyond the scope of this work.

NUMERICAL SIMULATIONS FOR LOCKING

Figs. 3(b) and 3(d), which show simulated results for master-slave locking of the two OMOs, are obtained by numerical integration of Eqs. S1 for each OMO. We perform the calculation using the solver *NDSolve* available in the commercial software Mathematica®.

Eqs. 1 are first solved for the master oscillator. Starting with initial values of $a_{master}(0) = 0, x_{master}(0) = 5 \cdot 10^{-12} m, \frac{dx_{master}}{dt} = 0$, the equations are integrated from $t_0 = 0$ to $t_{max} = 0.5ms$. We observe from the time trace of the solution that it takes about $0.1ms$ to reach steady-state oscillations. The time-dependent optical power transmitted from the master oscillator is stored in memory for later use.

$$P_{trans,master}(t) \propto |s_{0,master} - \sqrt{2\Gamma_{ex}} a_{master}(t)|^2 \tag{S17}$$

In the same way as for the master oscillator, Eqs. 1 are solved for the slave oscillator, at first without any coupling between the master and the slave. We observe that just like the master oscillator, the slave also takes about $100\mu s$ to reach steady-state oscillations. During the experiment, both the oscillators attain steady state oscillations before they are coupled together. To reflect this, the $s_{0,slave}$ is kept constant for $100\mu s$, before being modulated by $P_{trans,master}(t)$ (calculated earlier), as per Eq. S18. This is accomplished by using a Heaviside Step Function, with the argument $t_c = 100\mu s$, to couple the AC part of $P_{trans,master}(t)$ (Eq. S17) to s_{slave}. The DC part is filtered out so that only the RF oscillations, not the DC value of $P_{trans,master}(t)$, couple to s_{slave}, as in the experiment.

$$|s_{slave}(t)|^2 = |s_{0,slave}|^2 [1 + \mathcal{H}(t_c = 10^{-4}s) \cdot \frac{\Gamma}{2} \cdot (P_{trans,master}(t) - < P_{trans,master}(t) >)] \tag{S18}$$

Finally, Figs. 3(b) and 3(d) are obtained by calculating and plotting the PSD of $P_{trans,slave}(t)$ for increasing values of modulation strength Γ.

Note : Although it is not essential to let the oscillators reach steady state oscillations in simulations before coupling them, doing so gives results that match better with experiments. This is because optomechanical oscillators are highly nonlinear systems, and the limit-cycle in which they oscillate is dependent on initial conditions [12]. By ensuring that the oscillations reach steady state before coupling is switched on, the numerical calculations emulate experimental initial conditions better.

Time-dynamics of locking

When the modulation depth γ crosses the minimum value required to lock the slave oscillator to the master oscillator, the slave oscillator undergoes a change in its dynamics. This change, however, is not instantaneous. There is a period of transient behaviour before the frequency and amplitude of the slave oscillator settle at their new steady state values.

We can obtain a rough estimate of the duration of this transient behaviour from numerical simulation of Eqs. 1(a) and 1(b). First, we simulate oscillations of the master oscillator, and store the time-trace of $P_{trans,master}$ (Eq. S17). Then, we simulate for the slave oscillator, with $|s_{slave}|^2$ given by Eq. S18. In order to observe the locking-transients, the coupling between the master and the slave oscillators is 'switched-on' at $t = t_c$, using a Heaviside step-function $\mathcal{H}(t_c = 200\mu s)$. Note that although the individual oscillators reach steady-state oscillations after $100\mu s$, we simulate for an additional $100\mu s$ before coupling the slave oscillator to the master. This enables us to analyse the steady-state oscillations of the slave oscillator both before and after coupling to the master oscillator (see next paragraph).

Fig. S2(a) shows the time trace of $P_{trans,slave}$. It can be seen that the dynamics change almost instantly when coupling is switched on at $t = t_c = 200\mu s$. However, there are transients that persist, apparently until $t = 230\mu s$. This is better revealed in the Short-Time-Fourier-Transform (STFT) of the time trace in Fig. S2(b). The STFT gives the frequency spectrum of the signal within a specified window of time. In order to obtain Fig. S2(b) from Fig. S2(a), we calculate the frequency spectrum (Fig. S2(b), y-axis) using the FFT algorithm in discrete time-windows (Fig. S2(b), x-axis) that are $10\mu s$ long, with a $5\mu s$ overlap between adjacent windows. We see that the dominant frequency in the spectrum is 32.91MHz for $t \leq 200\mu s$, and it is 32.99MHz for $t \geq 230\mu s$. However, for $200\mu s \leq t \leq 230\mu s$, it can be seen that there is a transition between the two dominant frequencies.

PHASE NOISE OF THE LOCKED OSCILLATOR

Previous studies [13–15] have shown that the close-to-carrier phase noise of the locked slave oscillator is identical to that of the master oscillator. For a freely running oscillator, the phase noise is determined by the thermal noise affecting the oscillator [16]. The spring
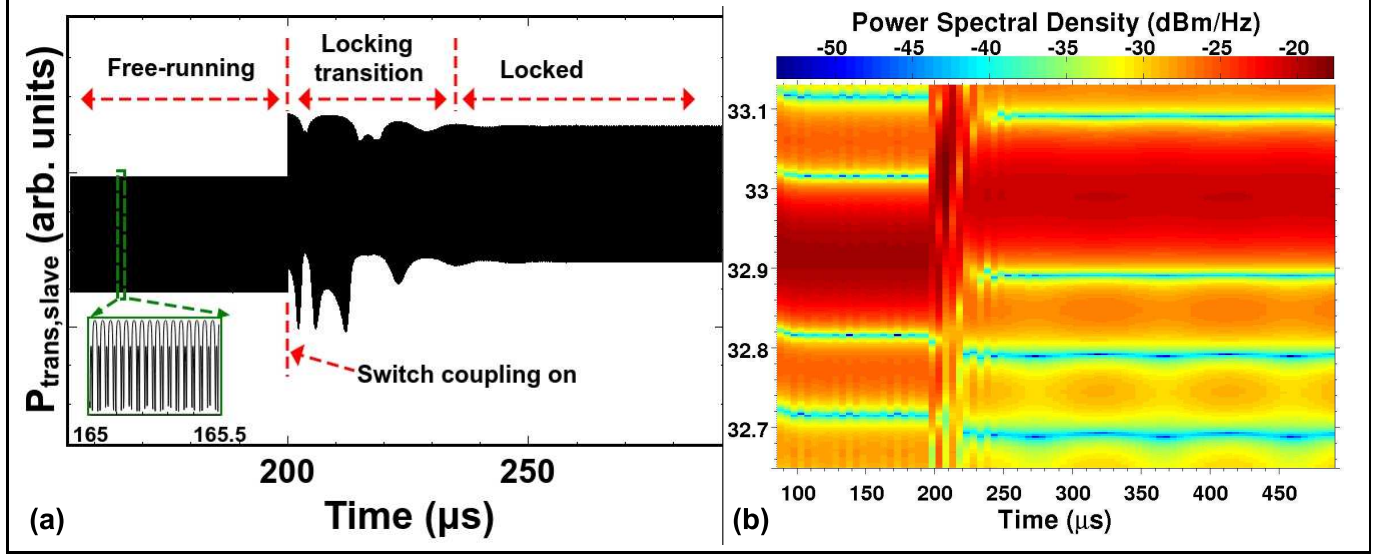
Figure S2. (a) Simulated time-trace of $P_{trans,slave}$. Inset shows a sample of the time-trace, showing the oscillating signal, over a few cycles. (b) The STFT of the signal from part (a), using $10\mu s$ long windows, and a time-step of $5\mu s$. The frequency resolution of the STFT is limited by the length of the window chosen for the STFT. A longer window would give better frequency resolution, at the expense of worse time-resolution.

constant of the resonator corresponds to a restoring force against perturbations to the amplitude, but there is no analogous restoring force for the phase i.e. phase perturbations add up [17]. When an external periodic force is introduced, it acts as a restoring force against phase perturbations, and serves to lock the phase of the slave to that of the master. This also results in the phase noise of the slave being identical to that of the master.

Fig. S3 shows the measured phase noise of master oscillator, and that of the slave oscillator before and after locking. It can be seen that the phase noise of the master oscillator is lower than that of the freely running slave oscillator. Upon locking, the phase noise of the slave reduces to a value close to, but slightly more than, that of the master. This difference can be attributed to the noise added by the photodetector, variable gain RF amplifier, and other electric circuitry in the path. It must be noted that this extra noise is small (e.g. 1.3dB at 50kHz offset). This implies that the use of a detector, RF amplifier and modulator in our scheme does not add a lot of noise and does not significantly raise the locking threshold (since noise influences the minimum injection ratio required for locking [17]).
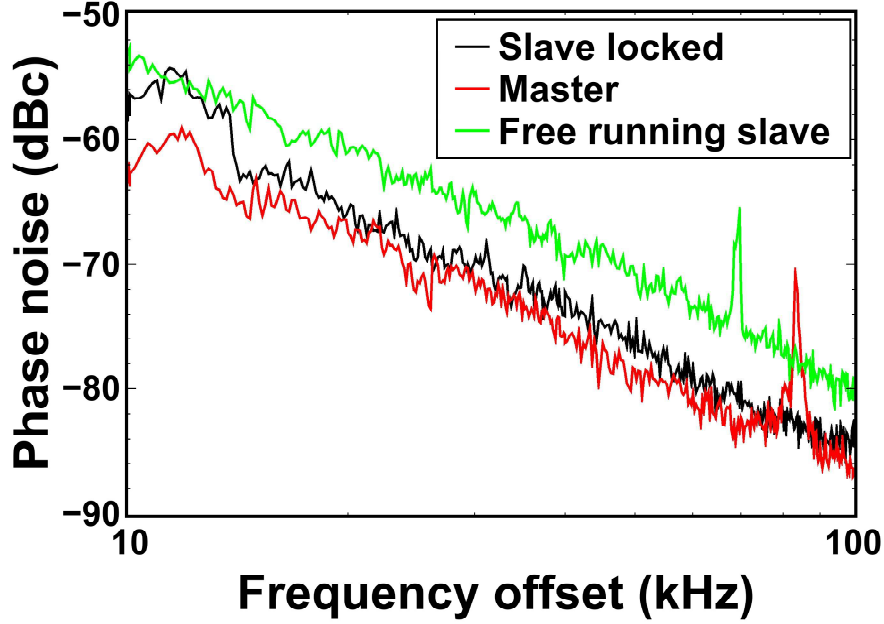
11

Figure S3. Phase noise of the master oscillator, and the slave oscillator (both freely running and locked). The spurious narrow peaks seen at 70kHz and 84kHz can be attributed to resonances of the tapered optical fibers used to excite the master and slave oscillators.

[1] H. A. Haus, *Waves and fields in optoelectronics* (Prentice Hall, Incorporated, 1984).

[2] T. J. Kippenberg and K. J. Vahala, Optics Express **15**, 17172 (2007).

[3] R. W. Boyd, *Nonlinear Optics* (Academic Press, 2008).

[4] M. Abramowitz and I. A. Stegun, *Handbook of Mathematical Functions: with Formulas, Graphs, and Mathematical Tables* (Courier Dover Publications, 2012).

[5] R. Adler, Proceedings of the IRE **34**, 351 (1946).

[6] B. Razavi, IEEE Journal of Solid-State Circuits **39**, 1415 (2004).

[7] R. H. Rand, *Lecture Notes on Nonlinear Vibrations*, Working Paper (2012) http://hdl.handle.net/1813/28989.

[8] M. Zhang, G. S. Wiederhecker, S. Manipatruni, A. Barnard, P. McEuen, and M. Lipson, Physical Review Letters **109**, 233906 (2012).

[9] $g_{om} = -2\pi 4.9 \times 10^{19} GHz/nm, \Gamma_{ex} = 5.138 \times 10^{8}/s, m_{eff} = 10^{-13} kg, \omega = 1.2037 \times 10^{15} rad/s, \Omega_m = 32.82 MHz, \Delta_0 = 4.856 \times 10^{9}/s, \Gamma_{opt} = 2.299 \times 10^{9}/s, s_0 = 10^{-4} W.$

[10] M. Zalalutdinov, K. L. Aubin, M. Pandey, A. T. Zehnder, R. H. Rand, H. G. Craighead, J. M. Parpia, and B. H. Houston, Applied Physics Letters **83**, 3281 (2003).

[11] M. Pandey, R. H. Rand, and A. T. Zehnder, Nonlinear Dynamics **54**, 3 (2008).

[12] F. Marquardt, J. G. E. Harris, and S. M. Girvin, Physical Review Letters **96**, 103901 (2006).

[13] K. Kurokawa, IEEE Transactions on Microwave Theory and Techniques **16**, 234 (1968).

[14] H.-C. Chang, X. Cao, M. Vaughan, U. K. Mishra, and R. York, IEEE Transactions on Microwave Theory and Techniques **45**, 2035 (1997).

[15] H.-C. Chang, X. Cao, U. K. Mishra, and R. York, IEEE Transactions on Microwave Theory and Techniques **45**, 604 (1997).

[16] H. Rokhsari, M. Hossein-Zadeh, A. Hajimiri, and K. Vahala, Applied Physics Letters **89**, 261109 (2006).

[17] A. Pikovsky and J. Kurths, *Synchronization: A Universal Concept in Nonlinear Sciences* (Cambridge University Press, 2003).